Egypt. J. Chem. **Vol. 66**, No. 11 pp. 77-91 (2023)

Egyptian Journal of Chemistry

http://ejchem.journals.ekb.eg/

Application of UV-A light Operating Photoreactor for Green Degradation of Direct Blue 15 through the Photo-Fenton-like process: Effects and Box-Behnken Optimization

Zainab A. Mahmoud[1*], Mohammed A. Atyia[1], Ahmed K. Hassan[2]

[1]*Al-Khwarizmi College of Engineering, University of Baghdad, Baghdad, Iraq.*

[2]*Environment and Water Directorate, Ministry of Science and Technology, Baghdad, Ira*

Abstract

In this research, green catalytic iron/copper nanoparticles loaded on bentonite were prepared by the green method using eucalyptus leaves extract as a reducing and capping agent (E-Fe/Cu@B-NPs). The characterization methods were employed on E-Fe/Cu@B-NPs, the NPs results were porous with a spherical shape when analysed by scanning electron microscopy (SEM), the BET analysis showed that the surface area of particles was 28.589m ^{2}/g. The functional groups of the E-Fe/Cu@B-NPs were also verified using Fourier transform infrared (FT-IR) spectroscopy. Degradation of direct blue 15 dye (DB15) was then investigated by E-Fe/Cu@B-NPs through photo-Fenton-like. The parameters such as pH, H_2O_2 dosage, initial DB15 concentration, and UV-intensity were studied through batch experiments and optimized through response surface methodology (RSM) using the Box-Behnken design (BBD). The results showed that the dye removal reached 100% within 60 minutes with optimum, pH 3.5, H_2O_2 dosage of 7.5 mmol/L, DB15 concentration 100 mg/L and UV-intensity of 15 W/m ^{2}. The kinetic study indicated that the DB15 degradation kinetic was fitted to the second-order kinetic model.

Keywords: Photo-Fenton-like; Box-Behnken design; Photoreactor design; Bentonite supported nanoparticles.

1. Introduction

During the last decades, huge growth occurs in the textile industry and the results of this growth started to affect the ecosystem dramatically [1]. where these industries produce large amounts of effluents containing organic dyes, especially azo dyes [2]. Direct discharge of these dyes into water bodies impacts on photosynthesis by disrupting the nitrogen and oxygen cycle, limiting the growth of organisms. This could have negative consequences for the food chain at present or in the immediate future [3]. Moreover, discharging these dyes into a water stream has negative effects on human health, even if these dyes are present in very low concentrations that do not exceed 1 ppm, because of the toxicity, mutagenic, and carcinogenic nature of these materials [3]. Accordingly, controlling this environmental pollutant becomes a challenge for many researchers.

Generally, physical, chemical, and biological methods such as coagulation, chemical oxidation, solvent extraction, membrane separation processes, catalytic degradation, and biodegradation (electrochemical, aerobic, and anaerobic) can be used to obtain water that meets the required specifications before it is released into the environment. However, these techniques are regarded as being costly, time-consuming, and producing a significant amount of secondary waste [4]. The promising techniques of advanced oxidation processes (AOPs) such as the Fenton-like process, photo-Fenton-like, and TiO_2-helped photocatalysis have recently been used as an alternative to traditional treatment methods due to their ability to degraded hazardous materials that are difficult to dispose of by traditional methods [5] .

The heterogeneous Fenton-like process involves in situ generation of the hydroxyl free radical (•OH) which has the ability to oxidize almost all organic compounds into CO_2, water, and inorganic ions [6]. The catalysts for hydrogen peroxide (H_2O_2) activation include zero-valent iron nanoparticles (ZVI-NPs) or transition metal-containing solids and the catalytic reactions are similar to homogeneous Fenton catalytic mechanisms, but only for reactions that take place on

*Corresponding author e-mail: Zainab.amahmoud@gmail.com;

Receive Date: 08 July 2022, Revise Date: 28 July 2022, Accept Date: 31 July 2022

DOI: 10.21608/EJCHEM.2022.149569.6463

the surface of heterogeneous catalysts, as described by (Eq. 1).

$Fe^{2+}+H_2O_2 \longrightarrow Fe^{3+} + \bullet OH + OH^-$ (1)

When ferric ions combine with the remaining H_2O_2, ferrous ions are regenerated, as shown in the equation below:

$Fe^{3+}+H_2O_2 \longrightarrow Fe^{2+}+H^++HO^{\bullet}_2$ (2)

A photochemical reaction in the photo-Fenton-like process can significantly boost the rate of pollutant degradation through several processes that occur simultaneously like photodegradation of dyes, and the photolysis of hydrogen peroxide. In this situation, a photoreduction mechanism is used to regenerate Fe^{2+}, resulting in the formation of more hydroxyl radicals as shown in (Eq. 3) [7].

$Fe(OH)^{2+} + hv \longrightarrow Fe^{2+} + \bullet OH$ (3)

Moreover, the nanoparticles (NPs) used as photo-Fenton-like catalysts can be prepared by chemical, physical, and biological techniques [8]. In any case, the biological method employing plant extract is preferable to the chemical and physical methods, as the chemical method uses some hazardous components as well as the complexity and expensive equipment used in the physical approach [9]. As a result, the environmentally friendly and affordable biological method of NPs preparation using plant extract can be carried out [10]. The plant extract contains many biomolecules like flavonoids, alkaloids, terpenoids, amides, aldehydes, and other biological constituents that can reduce the metal salts and produce zero-valent nanoparticles [11]. Moreover, the plant materials also can prevent the resultant NPs from agglomeration [12]. Despite many plant extracts being used for these purposes the eucalyptus leaf extract represent one of the good reductants and capping agents, besides the availability of this tree in Iraq and most countries [13].

ZVI-NPs prepared by green synthesis method received high attention recently due to several reasons; (1) increase the activity of this catalyst under light irradiation [14]; (2) the stability and reactivity of ZVI-NPs can be improved by anchoring the ZVI-NPs on a support material [15].

Furthermore, copper is one of the transition metals that can be used in calculated proportions with ZVI-NPs to prepare bimetallic nanoparticles (BMNPs). The idea of mixing the copper with iron is to enhance the generation of atomic hydrogen on the surface of BMNPs and therefore enhance the reductive degradation of dyes as well copper accelerates the galvanic corrosion of ZVI-NPs to generate Fe^{2+} as this ion reacts with H_2O_2 to generate •OH [16]. In addition, a wide variety of materials can be used as a support materials for NPs such as multi-walled carbon nanotubes, activated carbon, zeolite, bentonite clays [17], and kaolinite [18]. Particularly, bentonite exhibits good thermal, chemical, and mechanical stability and it also provides high specific surface area and is available at low cost [12]. No previous works have studied the catalytic ability of E-Fe/Cu@B-NPs through photo-Fenton-like reaction under different UV-A intensities.

The present study involved the design of photoreactor and employed the eucalyptus leaves extract to prepare bentonite-supported bimetallic nanoparticles (E-Fe/Cu@B-NPs) which in turn applied in the photo-Fenton-like process using UV-A light for degradation of direct blue 15 (DB15) dye from wastewater, the optimization of influencing parameters were performed through batch experiments using software design of experiments that was response surface methodology (RSM) based on Box-Behnken design (BBD).

2. Experimental work

2.1. Catalyst preparation

To prepare eucalyptus leaves extract, a 10 g of clean and dry leaves powder was added to 150 mL deionized water and boiled at 80 ℃ for 30 min. Some researchers have proven that a temperature of 80 ℃ is the best temperature at which most biochemical materials are obtained efficiently [19]. Once the extract was cooled

down, it was filtered using vacuum filtration to remove any suspended leaf particles. Thereafter, a quantity of 2 g of bentonite was added to 100 mL of deionized water and stirred for 30 min at room temperature. Meanwhile, 1.5 g Iron sulphate ($FeSO_4.7H_2O$) and 0.4 g of copper sulphate ($CuSO_4.5H_2O$) were dissolved separately each in 50 mL of deionized water. Then, the salts solutions were added to the bentonite solution and stirred for 60 min with an ultrasonic vibration water bath (Cole.Parmer. UK). To complete the E-Fe/Cu@B-NPs preparation, a 100 mL of eucalyptus extract was added slowly into the bentonite and salts mixture with constant stirring. After adding several drops of the extract, the colour of the mixture changed from yellow to black, indicating the reduction of Fe^{2+} and Cu^{2+} into zero-valent [20]. Thereafter, the black precipitate of E-Fe/Cu@B-NPs was separated by vacuum filtration. In addition, to prevent rapid oxidation of the NPs, the separated precipitate was washed directly with distilled water followed by absolute ethanol. The E-Fe/Cu@B-NPs were then dried overnight at room temperature and ground into a fine powder using mortar. Table 1 illustrates the source of materials used in catalyst preparation.

Table 1. Materials used in catalyst preparation and their sources.

Material	Source
Bentonite clay	State company of mining industry, department of mineral extraction, Iraq
($FeSO_4.7H_2O$)	Alpha chemical company
($CuSO_4.5H_2O$)	Romil LTD company

2.2. Characterization of E-Fe/Cu@B-NPs

The prepared E-Fe/Cu@B-NPs were characterized using different characterization methods to diagnose structure, morphology, specific surface area, size, and other important properties. The E-Fe/Cu@B-NPs size and shape were identified using scanning electron microscopy (SEM) and the latter is attached to an energy-dispersive X-ray spectroscopy (EDX) test that gives additional information about the chemical composition. In addition, the Brunauer, Emmett, and Teller (BET) analysis was used to determine specific surface area**,** pore size, and pore volume. Finally, the functional groups of E-Fe/Cu@B-NPs were analysed using Fourier transform infrared (FT-IR) spectroscopy.

2.3 Design of photoreactor

A piolet scale photoreactor was designed and operated using UV-A light as a radiation source. Different reaction capacity can be held out ranging between 2 L up to 5 L. 24 UV-A lamps (30 cm length, 2.2 cm width, power 8 W, and maximum wavelength peak of 365 nm) were fixed inside a cylindrical aluminium container of 40 cm diameter and 40 cm length to provide a reflective surface for incident photons inside the reactor, and each lamp supplies light with an intensity of 1 watt/m^2. The distance between the lamps and reaction cell adjusted to 10 cm and the distance between each lamp was 2.3 cm. Moreover, the aluminium container is fixed inside cubic wood (60×60×60 cm). Two fans mounted at the top of the photoreactor provides the cooling air to protect the reaction vessel from the hot lamp surfaces and the temperature inside the reactor does not exceed 30-40°C and these vans provide air circulation inside the reactor. The temperature inside the reaction cell and photoreactor was monitored using nine thermocouples evenly distributed inside the photoreactor. The configuration of the photoreactor is shown in Figure 1 and the schematic diagram of system is shown in Figure 2.

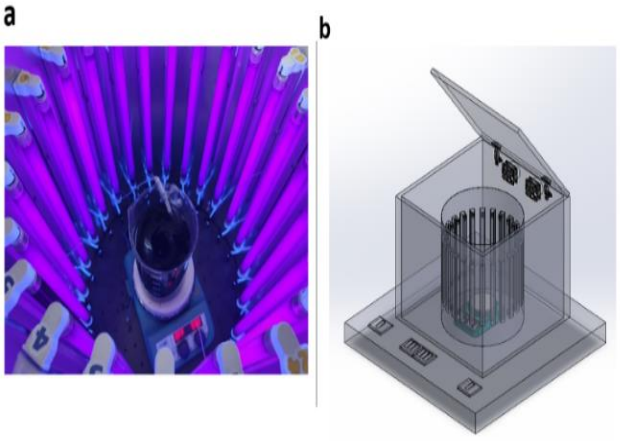

Figure 1. (a) image of batch photo-Fenton-like process inside photoreactor, (b) solid work configuration of photoreactor.

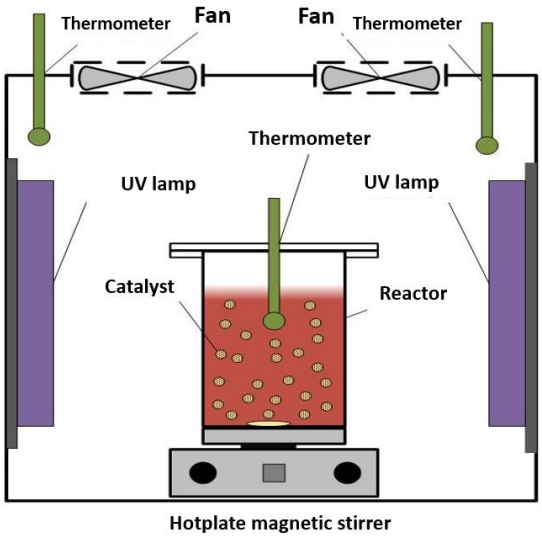

Figure 2. Schematic diagram of photoreactor.

2.4. Experimental design

The photo-Fenton-like experiments for DB15 removal were designed using RSM based on the 3-level 4-factor Box–Behnken experimental design. BBD through design expert software (version 13) [21]. Box–Behnken provides designs with the appropriate statistical features and the number of experiments needed for Box–Behnken design can be determined using the formula below

$$\boldsymbol{N = 2K(K-1) + CP} \qquad (4)$$

where k is the number of factors and cp is the number of central point replicates.

In addition, RSM is helpful to understand the effect of different parameters on response and interaction between independent variables through the analysis of variance (ANOVA). Additionally, the ANOVA provides an opportunity to analyse the data graphically and determines additional tools like probability (P-value) and Fisher-test (F-value), these terms indicate the significance of model and model terms. Whenever a P-value less than 5% with a high F-value indicates a significant effect on this term [22]. The coefficient of determination, R^2 examines the suitability of a polynomial model when the value of R^2 is close to one it indicates that the actual experiment results are close to the predicted one [23]. To prove that the adjusted and predicted responses are compatible, the difference between adjusted R^2 (R^2_{adj}) and predicted R^2 (R^2_{pre}) must be less than 0.2 [24]. Finally, the polynomial equation links the response with the independent variables that suggested by design software for the studied parameters shown in (Eq. 5) [5]. The studied parameters and their ranges are given in Table 2.

$$\boldsymbol{F(x) = \alpha_0 + \sum_{i=1}^{N} b_i x_i + \sum_{i=1}^{N} c_{ii} x_{2i} + \sum_{ij(i<j)}^{N} c_{ij} x_i x_j + \sum_{i=1}^{N} d_i x_{3i} + \sum_{i=1}^{N} e_i x_{4i}} \qquad (5)$$

Where N is the number of model inputs, $F(x)$ is the response, x_i is the set of model inputs, a_o is the constant coefficient, b_i and c_{ii}, are model coefficients, c_{ij} interaction coefficient, and i and j are 1, 2,3.

Table 2. Coded symbols and ranges for photo-Fenton-like process experiment parameters.

Parameters	Levels in Box–Behnken design		
	Low (-1)	**Middle (0)**	**High (+1)**
A: pH	2	3.5	5
B: H_2O_2 dosage (mmol/L)	0.5	4	7.5
C: DB15 concentration (mg/L)	15	57.5	100
D: UV-intensity (W/m^2)	6	15	24

Batch experiments were used to assess the degradation of DB15, and the reaction was carried out in a 1 L beaker. To prepare the dye solution, a stock solution of DB15 a concentration of 1000 mg/L was first prepared, and then different dye concentrations were diluted from this stock solution. The pH of the working solution was adjusted to the appropriate value using 1 M NaOH or 1 M H_2SO_4. Accordingly, 0.1 g of E-Fe/Cu@B-NPs were added to the dye solution [25] and magnetically stirred for 5 min in the dark to allow the NPs to be distributed homogeneously within the solution. Moreover, A predetermined amount of hydrogen peroxide (30% w/v) was added with the UV lamps turned on at the same time to initiate a photo-Fenton-like reaction. The reaction mixture was agitated with a magnetic stirrer at 300 rpm and at 35 ℃ for a predetermined period. During the experiments, approximately 8 mL of the reaction solution was sampled and filtered through a 0.45 µm syringe filter. The filtered solution was then placed into a 15 mL glass container filled with 200 µL of 1 M Na_2SO_3 solution and uniformly stirred to quench •OH. Finally, the samples were monitored by a UV/VIS-spectrophotometer (Shimadzu, UV-1800, Japan), and the dye removal efficiency was determined using (Eq. 6) [26].

$$\%\boldsymbol{DR} = \frac{\boldsymbol{C_o - C_t}}{\boldsymbol{C_o}} \times \boldsymbol{100} \qquad (6)$$

Where *%DR* is DB15 removal percentage, C_o is the initial DB15 concentration mg/L at t= 0, and C_t was the concentration of DB15 at time t min.

3. Results and discussion

3.1. Characterization of E-Fe/Cu@B-NPs

The SEM analysis in Figure 3 shows that the E-Fe/Cu@B-NPs were porous and shaped as spherical with a diameter ranging from (34.39-72.40 nm). Additionally, the homogeneous distribution of NPs on the surface of bentonite is shown [13].

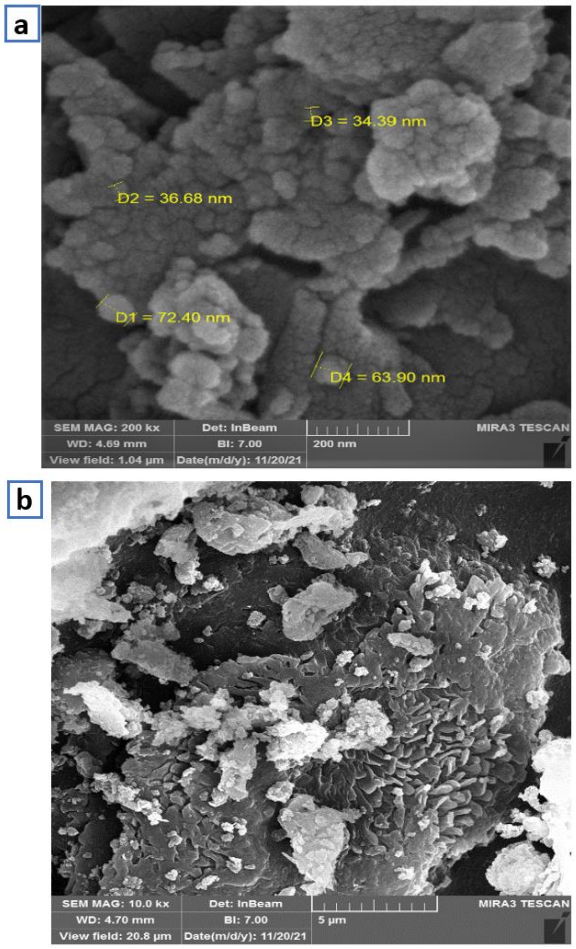

Figure 3. SEM images of E-Fe/Cu@B-NPs, (a) SEM MAG 200 kx, (b) SEM MAG 10 kx.

Moreover, the EDX analysis (Figure 4) illustrated the constituent of E-Fe/Cu@B-NPs, the chemical composition of E-Fe/Cu@B-NPs was demonstrated by the intense peaks of Fe, Cu, C, O, Si, Ne, Al, Mg, S, and Ca. However, C and O referred to the presence of polyphenols and other organic compounds in eucalyptus leaves extract [27]. Also, O could be referred to the oxide of elements for example Fe and Si [28]. Furthermore, the peaks Si, Al, Mg, S, Ne, and Ca appeared due to support the NPs on the calcium bentonite clay [13].

The specific surface area, pore size, and pore volume of E-Fe/Cu@B-NPs were analysed by BET analysis where the nitrogen (N_2) used as adsorptive at bath temperature of -196.87 ℃. The specific surface area, pore-volume, and pore size were 28.589 m^2/g, 0.063 cm^3/g, and 8 .861 nm, respectively. The results indicate that E-Fe/Cu@B-NPs consider mesoporous particles because pore size falls within the range (2-50 nm) [20]. The mesoporous pores along with a large specific surface area play an important role in the photo-Fenton-like process since the large surface area leads to enhancing catalytic effectiveness by increasing the amounts of reactants that move to the catalyst surface thereby developing the reaction time [29].

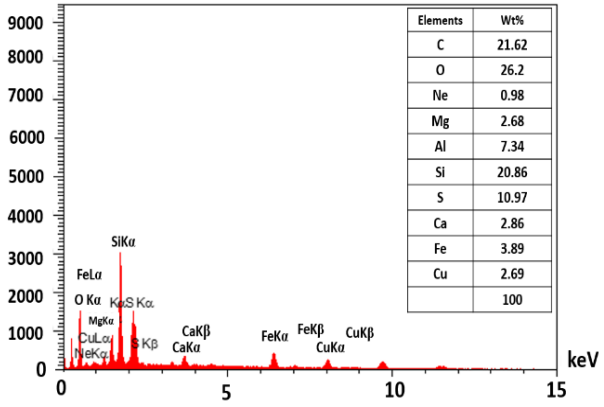

Figure 4. EDX of prepared E-Fe/Cu@B-NPs.

The functional groups of E-Fe/Cu@B-NPs were characterized by Fourier transform infrared (FT-IR) spectroscopy (Shimadzu, IRAffinity, Japan). The FT-IR spectra of the E-Fe/Cu@B-NPs in powdered form was recorded with a potassium bromide (KBr) pellet, and the analysis was performed using a mid-IR spectrum (400-4000cm^{-1}). As shown in (Figure 5).

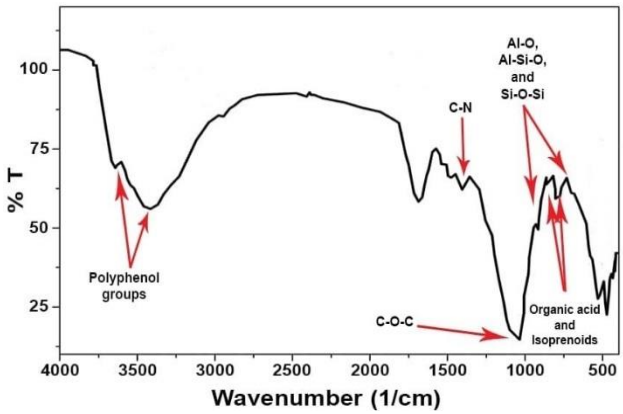

Figure 5. FT-IR of E-Fe/Cu@B-NPs.

The peaks near 3618 and 3406 cm^{-1} appeared because of the O-H stretching vibration, which indicates the presence of polyphenol groups that are capable of reducing Fe^{2+} and Cu^{2+} to Fe^{0} and Cu^{0} [30]. The peak at 1720 cm^{-1}, which is belonged to the C=C stretching vibration of the aromatic ring belonging to the non-saturated hydrocarbon compounds present in eucalyptus leaves [31]. Furthermore, the peaks in 1348 and 1039 cm^{-1} belong to C-N and C-O-C, respectively [19]. Similarly, peaks have been observed at 834 and 796 cm^{-1} belonging to organic acid and isoprenoids contained in eucalyptus extract [32]. These functional groups demonstrate the presence of a biomolecule in eucalyptus extract that plays an important role as a capping agent that prevents the agglomeration of NPs. The peaks between 522 – 438 cm^{-1} prove the existence of Fe/Cu NPs [33]. Due to the presence of bentonite, peaks at 918, 690.25, and 470.63 cm^{-1} were observed which belong to bending vibrations of Al-O, Al-Si-O, and Si−O−Si respectively.

3.2 Mathematical Model Fitting and ANOVA Analysis of Photo-Fenton-like Experiments

The experimental data obtain through photo-Fenton-like experiments analysed statistically by BBD and the adjusted and predicted values are listed in (Table 3). The R^2, (R^2_{adj}), (R^2_{pred}) and the stander deviation obtain from ANOVA analysis are listed in (Table 4). The high R^2 of the quadratic model indicate this model exhibits the best fit to experimental responses. Also, the R^2_{pred} is in reasonable agreement with the R^2_{adj} and the difference is less than 0.2 [34]. (Figure 6) showed the significance of the suggested model by the plot of the experimental versus predicted values which represents a suitable tool in studying the significance of the suggested model. According to ANOVA analysis (Table 4), the model F-value and P-value were 223.3and < 0.0001, respectively, which indicates the model is significant.

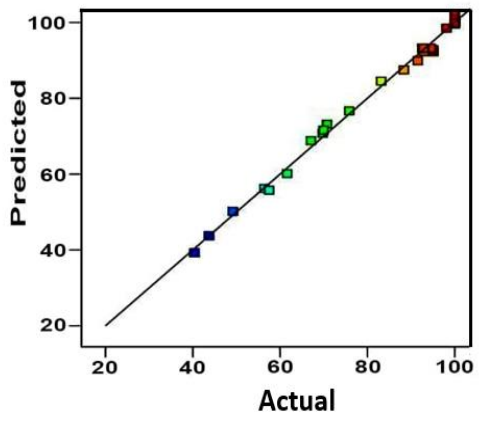

Figure 6. Actual versus predicted responses.

Furthermore, the sum of squares of studied parameters indicated that the pH was the parameter that had the greatest impact, followed by the H_2O_2 dosage and DB15 concentration, while UV intensity had the least effect on DB15 degradation. Additionally, the term BC, which denotes the interaction between H_2O_2 dosage and DB15 concentration, significantly affects the efficiency of DB15 removal. The quadratic model for DB15 removal is given in (Eq. 7).

$$\%DR = 27.624 + 46.667A + 4.899B - 0.38C + 0.641D - 0.381AB - 0.064AC + 0.06BC + 0.054BD + 0.0048CD - 8.019A^2 - 0.533B^2 - 0.0377D^2 \quad (7)$$

3.3. Kinetic study and effect of parameters in the batch mode

Three kinetic models including zero, first, and second-order kinetic models were used to assess the speed of a photo-Fenton-like process based on the initial DB15 concentration and the DB15 concentration after a certain duration. Moreover, the removal kinetics of DB15 were studied at the various experimental conditions such as pH, H2O2 dosage, DB15 concentration, and UV-intensity. The correlation coefficients R^2 for all parameters along with ko, k1, and k2, were determined based on the best fit of the kinetic model to experimental data using kinetic models as illustrate in the below equations [27]. The parameters of kinetic models and the corresponding correlation coefficients for all parameters are shown in (Table 5).

Zero-order $Ct = Co - kot$ (8)

First-order $\ln Ct = \ln C1 - k1t$ (9)

Second-order $\frac{1}{Ct} - \frac{1}{Co} = k2t$ (10)

Where ko, k1, and k2 are reaction rate constants of zero, first, and second-order reaction kinetics respectively. The linear fitting of kinetic models are show in Figures (7, 8, 9) and the second-order kinetic model was the most fitted model for DB15 degradation by photo-Fenton-like reaction.

Table 3. Box-Behnken design of batch experiments with actual and predicted responses.

EXP.	A: pH	B: H_2O_2 dosage (mmol/L)	C: DB15 conc. (mg/L)	D: UV-intensity (W/m^2)	Actual Value %	Predicted Value %
1	3.5	4	57.5	15	92.56	93.23
2	3.5	0.5	57.5	6	69.77	70.79
3	5	4	57.5	6	49.19	50.16
4	3.5	4	15	6	100	99.56
5	5	4	57.5	24	56.41	56.20
6	3.5	4	100	24	83.14	84.53
7	3.5	0.5	57.5	24	69.97	71.60
8	2	4	15	15	100	100
9	3.5	4	57.5	15	92.98	93.23
10	3.5	4	100	6	75.85	76.66
11	2	4	100	15	88.35	87.49
12	3.5	7.5	57.5	6	93	92.28
13	5	0.5	57.5	15	40.37	39.26
14	3.5	7.5	15	15	100	99.88
15	3.5	4	15	24	100	100
16	5	4	100	15	43.69	43.73
17	3.5	7.5	100	15	98.13	98.49
18	3.5	4	57.5	15	92.87	93.23
19	5	4	15	15	67.07	68.84
20	2	7.5	57.5	15	100	100
21	2	0.5	57.5	15	70.75	73.15
22	5	7.5	57.5	15	61.6	60.14
23	2	4	57.5	6	91.51	89.88
24	3.5	0.5	15	15	95.05	92.84
25	3.5	4	57.5	15	94.5	93.23
26	2	4	57.5	24	95.1	92.28
27	3.5	0.5	100	15	57.48	55.75
28	3.5	7.5	57.5	24	100	99.89

Table 3. ANVOA for the quadratic model for batch experiments

Source	Sum of Squares	df	Mean Square	F-value	p-value	
Model	9851.7	10	985.1	223.3	< 0.0001	significant
A-pH	4308.5	1	4308.5	976.5	< 0.0001	
B H2O2 dosage	1858.5	1	1858.5	421.2	< 0.0001	
C- dye conc.	1111.3	1	1111.3	251.9	< 0.0001	
D- UV intensity	53.34	1	53.3	12.1	0.0029	
AB	16.1	1	16.1	3.6	0.0733	
AC	34.4	1	34.4	7.8	0.0125	
BC	318.6	1	318.6	72.2	< 0.0001	
A^2	2086.3	1	2086.3	472.8	< 0.0001	

B^2	274.2	1	274.2	62.1	< 0.0001	
D^2	60.2	1	60.2	13.7	0.0018	
Residual	75	17	4.			
Lack of Fit	72.8	14	5.20	6.9	0.0685	not significant
Pure Error	2.3	3	0.75			
Cor Total	9926.8	27				
R^2	0.995					
Adjsted R^2	0.99					
Predicted R^2	0.98					
Adeq. precision	50.39					
Std. Dev.	1.83					

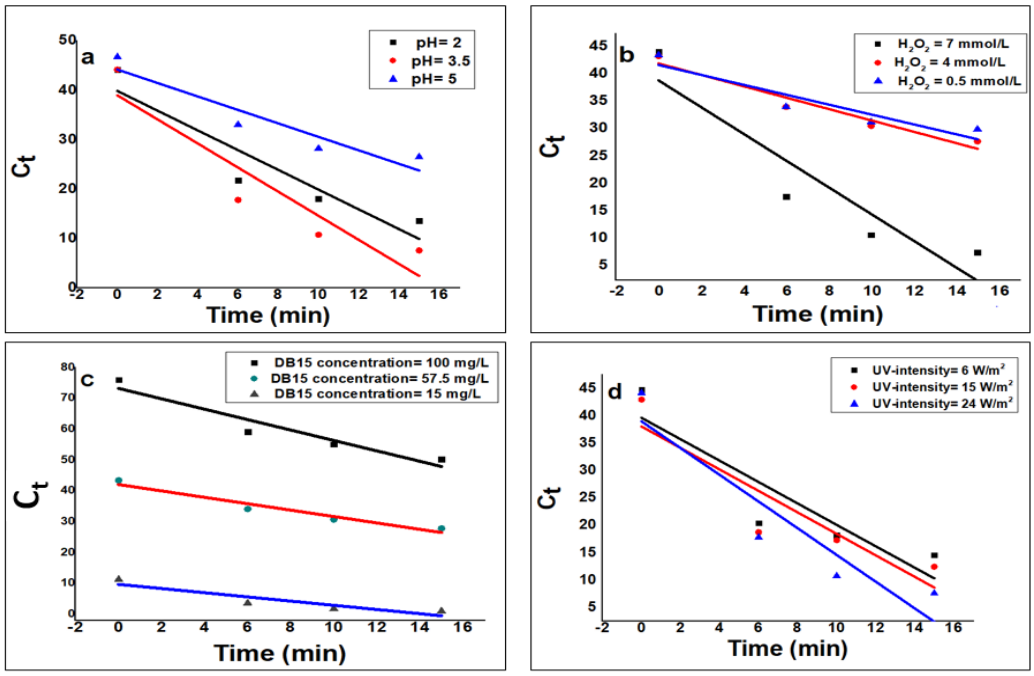

Figure 7. Linear regression for zero-order kinetic of DB15 degradation. (a): pH, (b) H_2O_2 dosage, (c): Dye concentration, and (d): UV-intensity.

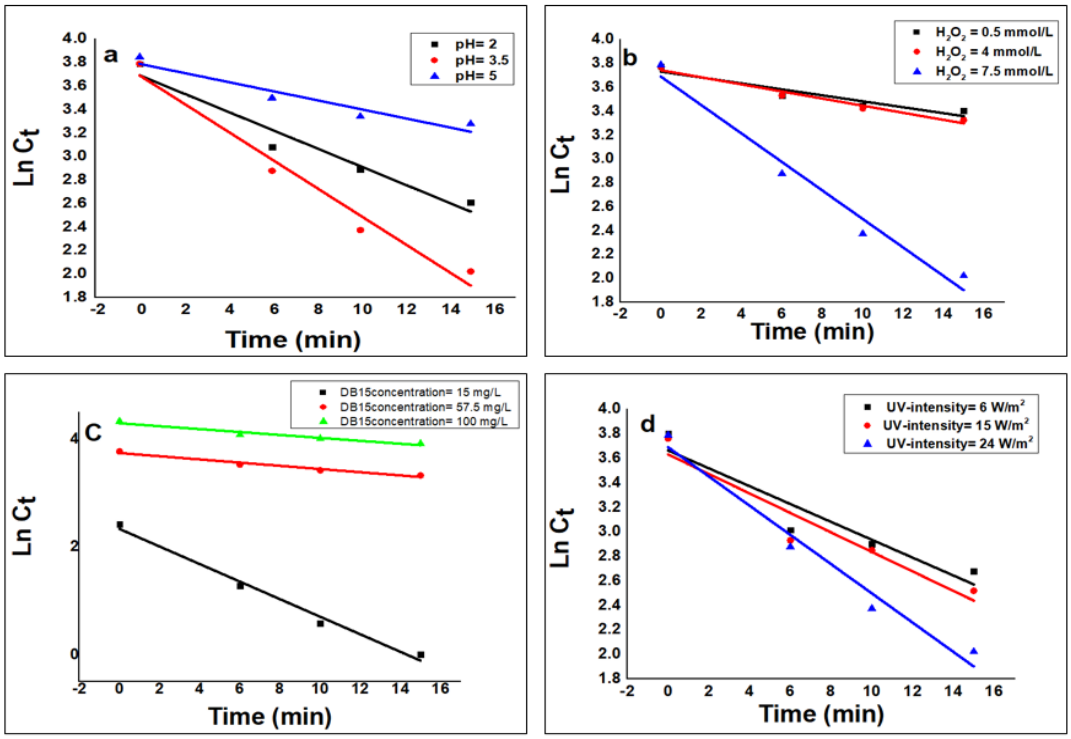

Figure 8. Linear regression for first-order kinetic of DB15 degradation. (a): pH, (b) H_2O_2 dosage, (c): Dye concentration, and (d): UV-intensity

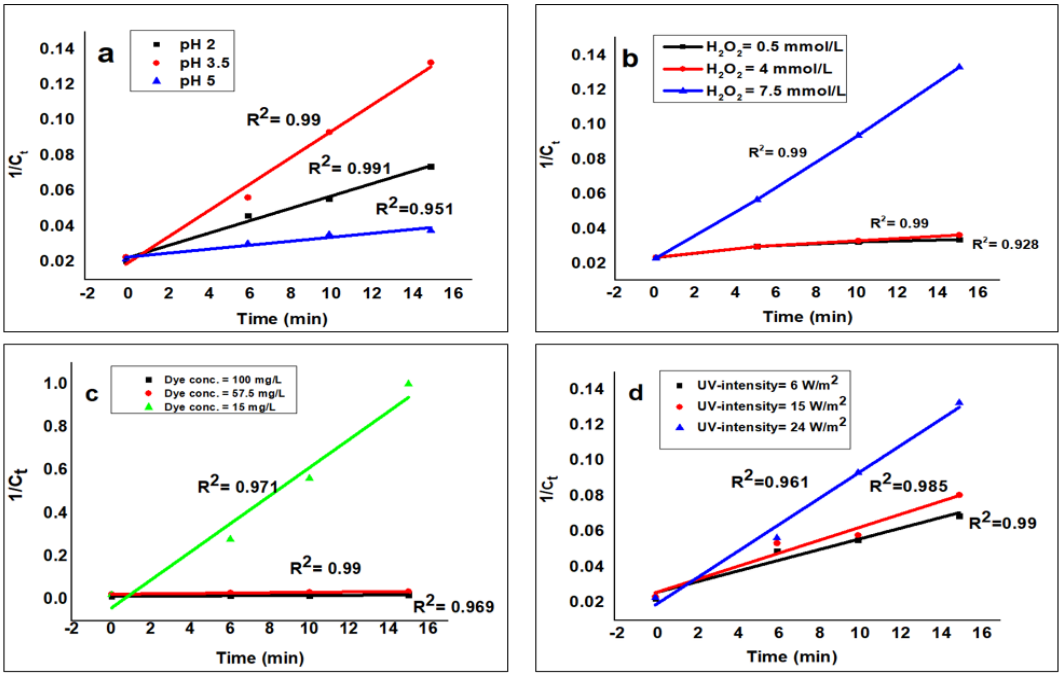

Figure 9. Linear regression for second-order kinetic of DB15 degradation. (a): pH, (b) H_2O_2 dosage, (c): Dye concentration, and (d): UV-intensity.

Table 5. The kinetics constants and regression coefficient of Zero, First, and Second-order models for degradation DB15.

Parameters		Zero-order		First-order		Second-order	
		K_o	R^2	K_1 (min^{-1})	R^2	K_2 ($mg^{-1}min^1$)	R^2
pH	2	1.35	0.848	0.0641	0.983	0.0035	0.991
	3.5	2.598	0.867	0.093	0.972	0.0049	0.99
	5	1.362	0.887	0.036	0.939	0.0011	0.951
Average R^2			0.867		0.965		0.977
H_2O_2 (mmol/L)	0.5	0.8237	0.7935	0.025	0.907	0.0007	0.928
	4	1.0377	0.945	0.0297	0.97	0.0009	0.99
	7.5	2.598	0.8665	0.093	0.972	0.0049	0.99
Average R^2			0.868		0.950		0.969
Dye concentration (mg/L)	15	0.615	0.753	0.163	0.987	0.065	0.971
	57.5	1.038	0.945	0.093	0.970	0.001	0.99
	100	1.688	0.919	0.027	0.947	0.0004	0.969
Average R^2			0.872		0.968		0.977
UV-intensity (W/m^2)	6	1.742	0.702	0.073	0.893	0.003	0.961
	15	1.959	0.828	0.098	0.912	0.004	0.985
	24	2.598	0.8665	0.093	0.972	0.005	0.99
Average R^2			0.799		0.926		0.979
Average R^2			0.852		0.952		0.976

3.3.1 Effect of pH

In photo-Fenton-like process pH consider important parameter and affect H_2O_2 stability. As shown in Figure 10 total colour removal was observed at pH (2.5-3.5). The removal efficiency decreased when pH decreased from 2.5 to 2. Also, the reaction constant k_2 was 0.0035 and 0.0049 $mg^{-1}min^{-1}$ at pH 2 and 3.5 respectively. This phenomenon occurred due to the formation of an oxonium ion (H_3O^{2+}) which promote the stability of H_2O_2 and leads to inhibition of •OH generation [35]. Additionally, when the pH increased from 3.5 to 5 the removal efficiency was greatly lessened, and the reaction was slow with k_2 0.0011 $mg^{-1}min^{-1}$. This effect caused by the synthesis of an iron hydroxide complex, which cause the decomposition of H_2O_2 into water and oxygen [36]. However, pH 3.5 considers optimum for the photo-Fenton-like process.

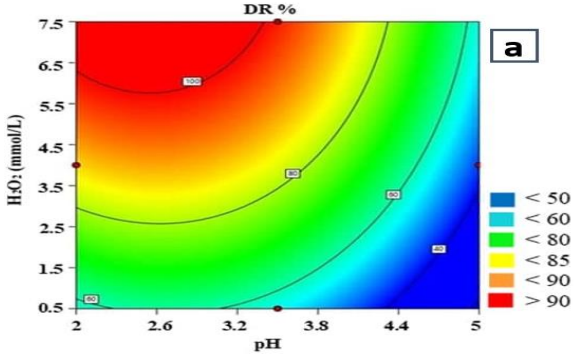

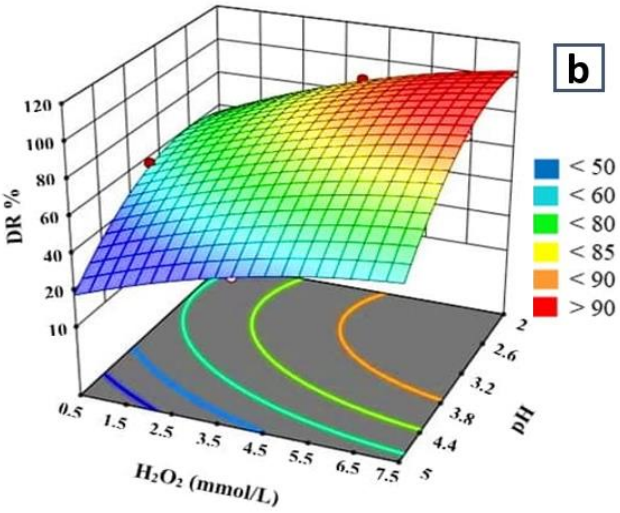

Figure 10. Interaction effect of pH and H_2O_2 dosage of the DB15 degradation at UV intensity 15 W/m^2 and DB15 concentration 100 mg/L, (a) contour plot (b) 3D surface.

3.3.2 Interaction effect of DB15 concentration and H_2O_2 dosage

According to ANOVA analysis (Table 3), the dye concentration has a significant effect on DB15 removal. As shown in (Table 4), k_2 decreased from (0.065 to 0.0004 $mg^{-1}min^{-1}$) when dye concentration increased from (15 to 100 mg/L). Figure 11 shows that the removal efficiency was also decreased with rising DB15 concentration. Because •OH generation is reduced under high dye concentrations due to blocking of catalyst active site by dye molecules and prevent H_2O_2 catalysis [37]. Additionally, dye molecules serve as light filters to inhibit H_2O_2 decomposition and stop catalysts from being activated by light [37].

Furthermore, hydrogen peroxide is an important parameter and essential source of oxidizing radicles so must be maintained at an optimum level to avoid the scavenging effect of high H_2O_2 dosage. According to Figure 11, increasing in H_2O_2 dosage leads to rising degradation efficiency due to availability of sufficient oxidizing agent •OH [38]. The k_2 increased from (0.0007 to 0.0049 $mg^{-1}min^{-1}$) when the H_2O_2 dosage increased from (0.5 to 7.5 mmol/L). As results the H_2O_2 dosage 7.5 mmol/L was considered as the best peroxide dosage. Furthermore, the interaction effect between H_2O_2 dosage and dye concentration has a P-value <0.0001, showing that there was a significant interaction between these two parameters. This interaction was evident since even a small amount of peroxide induced noticeable removal at a dye concentration of 15 mg/L.

3.3.3 Effect of UV intensity

As shown in Figure 12 increasing the UV intensity from (6 – 24 W/m^2) lead to rising the degradation efficiency and k_2 slightly increased. These phenomena occur due to faster photolysis of the H_2O_2 as shown in Eq. 11. Also, reduction of Fe^{+3} complex and regeneration Fe^{+2} take place under UV illustrated in Eq. 12 [39].

$$H_2O_2 + h\nu \rightarrow 2HO^{\bullet} \quad (11)$$

$$FeOOH^{+2} + h\nu \rightarrow Fe^{+2} + HO_2\bullet \quad (12)$$

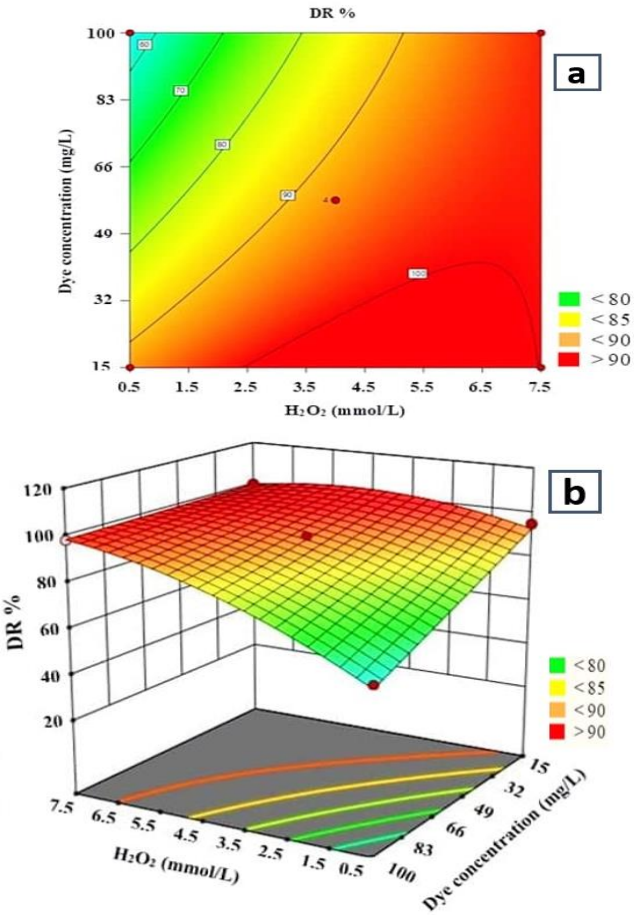

Figure 11. Interaction effect of DB15 concentration and H_2O_2 dosage on the DB15 degradation at UV intensity 15 W/m^2 and pH 3.5 (a) contour plot (b) 3D surface.

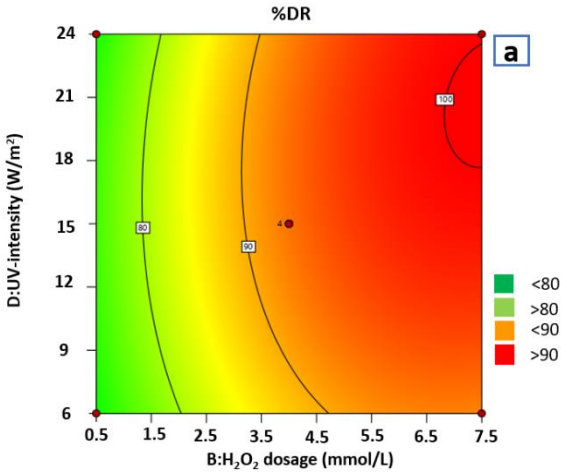

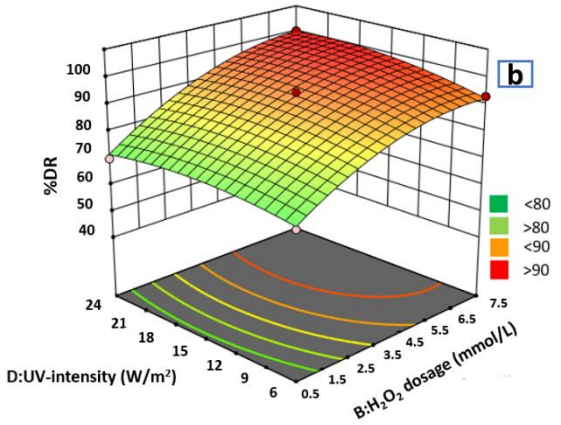

Figure 12. Interaction effect of UV intensity and H_2O_2 dosage at pH 3.5 and DB15 concentration 57.5 mg/L (a) contour plot (b) 3D surface.

3.4. Optimum conditions and conformation

Based on the response optimization of the design expert the conditions in (Table 6) have been obtained as optimum conditions. Also, the conformation experiments have been conducted as shown in (Table 7)

Table 6. Optimum conditions obtained by BBD.

Parameters	pH	H_2O_2 dosage (mmol/L)	DB15 concentration (mg/L)	UV-intensity (W/m^2)
Optimum conditions	3.5	7.5	100	15
Removal efficiency (%)	100			

Table 7. The results of conformation experiments

EXP.	Parameters			
EXP.1	pH	H_2O_2 dosage (mmol/L)	DB15 concentration (mg/L)	UV-intensity (W/m^2)
	3.5	7.5	100	15
Removal efficiency (%)	99.5%			
EXP.2	pH	H_2O_2 dosage (mmol/L)	DB15 concentration (mg/L)	UV-intensity (W/m^2)
	3.5	7.5	100	15
Removal efficiency (%)	98.3%			

4. CONCLUSION

The green synthesis approach was used to prepared iron/copper nanoparticles that were successfully loaded onto bentonite. The developed catalyst was then used to examine direct blue 15 (DB15) degradation via the photo-Fenton-like process. The photo-Fenton-like process was carried out in specially designed photoreactor using UV-A light. The results showed that the UV-A light has a good effect on the catalyst performance and the DB15 was completely removed after 60 min. Additionally, The DB15 degradation kinetics by photo-Fenton-like process were fitted to the second-order kinetic model with regression coefficient of R^2 0.976. Finally, the model equation for DB15 removal through photo-Fenton-like process is expressed by equation below:

$$\%DR = 27.624 + 46.667A + 4.899B - 0.38C + 0.641D - 0.381AB - 0.064AC + 0.06BC + 0.054BD + 0.0048CD - 8.019A^2 - 0.533B^2 - 0.0377D^2$$

5. ACKNOWLEDGEMENTS

The authors are highly indebted to the Department of Biochemical Engineering/al-Khwarizmi College of Engineering at the University of Baghdad, Iraq, and the Environment and Water Directorate of the Ministry of Science and Technology, Iraq, for providing all the facilities to carry out this work.

References

[1] R. A. Putri, S. Safni, N. Jamarun, and U. Septiani, "Kinetics study and degradation pathway of methyl orange photodegradation in the presence of C-N-codoped TiO2 catalyst," *Egypt. J. Chem.*, vol. 63, no. Part 2, pp. 563–575, 2020, doi: 10.21608/ejchem.2019.14543.1883.

[2] N. C. Fernandes *et al.*, "Removal of azo dye using Fenton and Fenton-like processes: Evaluation of process factors by Box–Behnken design and ecotoxicity tests," *Chem. Biol. Interact.*, vol. 291, pp. 47–54, 2018, doi: 10.1016/j.cbi.2018.06.003.

[3] J. Khan *et al.*, "Kinetic and thermodynamic study of oxidative degradation of acid yellow 17 dye by Fenton-like process: Effect of HCO3−, CO32−, Cl− and SO42− on dye degradation," *Bull. Chem. Soc. Ethiop.*, vol. 33, no. 2, pp. 243–254, 2019, doi: 10.4314/bcse.v33i2.5.

[4] A. G. Trovó, A. K. Hassan, M. Sillanpää, and W. Z. Tang, "Degradation of Acid Blue 161

by Fenton and photo-Fenton processes," *Int. J. Environ. Sci. Technol.*, vol. 13, no. 1, pp. 147–158, 2016, doi: 10.1007/s13762-015-0854-6.

[5] A. M. Tayeb, M. A. Tony, and S. A. Mansour, "Application of Box–Behnken factorial design for parameters optimization of basic dye removal using nano-hematite photo-Fenton tool," *Appl. Water Sci.*, vol. 8, no. 5, pp. 1–9, 2018, doi: 10.1007/s13201-018-0783-x.

[6] M. Solís-López, A. Durán-Moreno, F. Rigas, A. A. Morales, M. Navarrete, and R. M. Ramírez-Zamora, "Assessment of Copper Slag as a Sustainable Fenton-Type Photocatalyst for Water Disinfection," *Water Reclam. Sustain.*, pp. 199–227, 2014, doi: 10.1016/B978-0-12-411645-0.00009-2.

[7] T. Qureshi, M. Bakhshpour, K. Çetin, A. A. Topçu, and A. Denizli, "Wastewater Treatment : Synthesis of Effective Photocatalysts Through Novel Approaches HF Hydrogen fluoride," in *Photocatalysts in Advanced Oxidation Processes for Wastewater Treatment*, 2020, pp. 33–64.

[8] A. K. Hassan, M. A. Atiya, and I. M. Luaibi, "A Green Synthesis of Iron / Copper Nanoparticles as a Catalytic of Fenton-like Reactions for Removal of Orange G Dye Abstract : Introduction : Materials and Methods :," no. May, pp. 1249–1264, 2022.

[9] K. Vijayaraghavan and T. Ashokkumar, "Plant-mediated biosynthesis of metallic nanoparticles: A review of literature, factors affecting synthesis, characterization techniques and applications," *J. Environ. Chem. Eng.*, vol. 5, no. 5, pp. 4866–4883, 2017, doi: 10.1016/j.jece.2017.09.026.

[10] M. ; Kadhim, Fatimah; Atiya and A. Hassan, "Green Synthesis of Silver Nanoparticle Using Green Tea Leaves Extract for Removal Ciprofloxacin (Cip) From Aqueous Media," *Int. J. Res. Med. Sci. Technol.*, vol. 11, no. 1, pp. 74–99, 2021, doi: 10.37648/ijrmst.v11i01.008.

[11] A. S. Abdelbaky and Y. M. Diab, "Effect of Various Extraction Methods and Solvent Types on Yield, Phenolic and Flavonoid Content and Antioxidant Activity of Spathodea nilotica Leaves," *Egypt. J. Chem.*, vol. 64, no. 12, pp. 7483–7489, 2021, doi: 10.21608/EJCHEM.2021.96557.4518.

[12] T. Bao *et al.*, "Bentonite-supported nano zero-valent iron composite as a green catalyst for bisphenol A degradation: Preparation, performance, and mechanism of action," *J. Environ. Manage.*, vol. 260, no. October 2019, 2020, doi: 10.1016/j.jenvman.2020.110105.

[13] K. Sravanthi, D. Ayodhya, and P. Y. Swamy, "Green synthesis, characterization and catalytic activity of 4-nitrophenol reduction and formation of benzimidazoles using bentonite supported zero valent iron nanoparticles," *Mater. Sci. Energy Technol.*, vol. 2, no. 2, pp. 298–307, 2019, doi: 10.1016/j.mset.2019.02.003.

[14] A. Mossmann, G. L. Dotto, D. Hotza, S. L. Jahn, and E. L. Foletto, "Preparation of polyethylene-supported zero-valent iron buoyant catalyst and its performance for Ponceau 4R decolorization by photo-Fenton process," *J. Environ. Chem. Eng.*, vol. 7, no. 2, p. 102963, 2019, doi: 10.1016/j.jece.2019.102963.

[15] M. Alizadeh, Fard, A. Torabian, G. R. N. Bidhendi, and B. Aminzadeh, "Fenton and Photo-Fenton Oxidation of Petroleum Aromatic Hydrocarbons Using Nanoscale Zero-Valent Iron," *J. Environ. Eng.*, vol. 139, no. 7, pp. 966–974, 2013, doi: 10.1061/(asce)ee.1943-7870.0000705.

[16] R. Yamaguchi, S. Kurosu, and M. Suzuki, "Hydroxyl radical generation by zero-valent iron/Cu (ZVI/Cu) bimetallic catalyst in wastewater treatment: Heterogeneous Fenton/Fenton-like reactions by Fenton reagents formed in-situ under oxic conditions," *Chem. Eng. J.*, vol. 334, pp. 1537–1549, 2018, doi: 10.1016/j.cej.2017.10.154.

[17] A. E. Elsayed *et al.*, "Synthesis of super magnetite(Fe3O4)/ bentonite nanocomposite for efficient remediation for industrial wastewater effluents," *Egypt. J. Chem.*, vol. 63, no. 12, pp. 5011–5026, 2020, doi: 10.21608/ejchem.2020.27520.2574.

[18] K. Babak, A. Takdastan, S. Pourfadakari, M. Ahmadmoazzam, and S. Jorfi, "Heterogeneous catalytic degradation of organic compounds using nanoscale zero-valent iron supported on kaolinite: Mechanism, kinetic and feasibility studies," *J. Taiwan Inst. Chem. Eng.*, vol. 96, no. January, pp. 329–340, 2019, doi: 10.1016/j.jtice.2018.11.027.

[19] R. Hao, D. Li, J. Zhang, and T. Jiao, "Green synthesis of iron nanoparticles using green tea and its removal of hexavalent chromium," *Nanomaterials*, vol. 11, no. 3, pp. 1–13, 2021, doi: 10.3390/nano11030650.

[20] I. M. Luaibi, M. A. Atiya, A. K. Hassan, and Z. A. Mahmoud, "Heterogeneous catalytic degradation of dye by Fenton-like oxidation over a continuous system based on Box–Behnken design and traditional batch

experiments," *Karbala Int. J. Mod. Sci.*, vol. 8, no. 2, pp. 9–28, 2022, doi: 10.33640/2405-609x.3217.

[21] Y. N. Kanafin, A. Makhatova, V. Zarikas, E. Arkhangelsky, and S. G. . Poulopoulos, "Photo-fenton-like treatment of municipal wastewater," *Catalysts*, vol. 11, no. 10, 2021, doi: 10.3390/catal11101206.

[22] S. C. Azimi, F. Shirini, and A. Pendashteh, "Treatment of wood industry wastewater by combined coagulation–flocculation–decantation and fenton process," *Water Environ. Res.*, vol. 93, no. 3, pp. 433–444, 2021, doi: 10.1002/wer.1441.

[23] D. Solomon, Z. Kiflie, and S. Van Hulle, "Using Box–Behnken experimental design to optimize the degradation of Basic Blue 41 dye by Fenton reaction," *Int. J. Ind. Chem.*, vol. 11, no. 1, pp. 43–53, 2020, doi: 10.1007/s40090-020-00201-5.

[24] M. H. Marzbali and M. Esmaieli, "Fixed bed adsorption of tetracycline on a mesoporous activated carbon: Experimental study and neuro-fuzzy modeling," *J. Appl. Res. Technol.*, vol. 15, no. 5, pp. 454–463, 2017, doi: 10.1016/j.jart.2017.05.003.

[25] J. Das and S. S. Dhar, "Camellia sinensis mediated synthesis of zero valent iron nanoparticles and study of their efficacy in dye degradation and antibacterial activity," *Int. J. Environ. Anal. Chem.*, vol. 00, no. 00, pp. 1–14, 2020, doi: 10.1080/03067319.2020.1828388.

[26] M. A. Atiya, A. K. Hassan, and F. Q. Kadhim, "Green synthesis of iron nanoparticle using tea leave extract for removal ciprofloxacin (CIP) from aqueous medium," *J. Eng. Sci. Technol.*, vol. 16, no. 4, pp. 3199–3221, 2021.

[27] X. Weng, M. Guo, F. Luo, and Z. Chen, "One-step green synthesis of bimetallic Fe/Ni nanoparticles by eucalyptus leaf extract: Biomolecules identification, characterization and catalytic activity," *Chem. Eng. J.*, vol. 308, pp. 904–911, 2017, doi: 10.1016/j.cej.2016.09.134.

[28] A. K. Hassan, G. Y. Al-Kindi, and D. Ghanim, "Green synthesis of bentonite-supported iron nanoparticles as a hetrogenous Fenton-like catalyst kinetic of decolorization of reactive blue 238 dye." Water Science and Engineering, Iraq, 2020, doi: 10.1016/j.wse.2020.12.001.

[29] J. Wang and J. Tang, "Fe-based Fenton-like catalysts for water treatment: Preparation, characterization and modification," *Chemosphere*, vol. 276, p. 130177, 2021, doi: 10.1016/j.chemosphere.2021.130177.

[30] K. Ramar, A. J. Ahamed, and K. Muralidharan, "Robust green synthetic approach for the production of iron oxide nanorods and its potential environmental and cytotoxicity applications," *Adv. Powder Technol.*, vol. 30, no. 11, pp. 2636–2648, 2019, doi: 10.1016/j.apt.2019.08.011.

[31] Y. Liu, X. Jin, and Z. Chen, "The formation of iron nanoparticles by Eucalyptus leaf extract and used to remove Cr(VI)," *Sci. Total Environ.*, vol. 627, pp. 470–479, 2018, doi: 10.1016/j.scitotenv.2018.01.241.

[32] M. Fazlzadeh, K. Rahmani, A. Zarei, H. Abdoallahzadeh, F. Nasiri, and R. Khosravi, "A novel green synthesis of zero valent iron nanoparticles (NZVI) using three plant extracts and their efficient application for removal of Cr(VI) from aqueous solutions," *Adv. Powder Technol.*, vol. 28, no. 1, pp. 122–130, 2017, doi: 10.1016/j.apt.2016.09.003.

[33] G. Gopal, H. Sankar, C. Natarajan, and A. Mukherjee, "Tetracycline removal using green synthesized bimetallic nZVI-Cu and bentonite supported green nZVI-Cu nanocomposite: A comparative study," *J. Environ. Manage.*, vol. 254, no. June 2019, p. 109812, 2020, doi: 10.1016/j.jenvman.2019.109812.

[34] Q. Zhao, J. F. Kennedy, X. Wang, X. Yuan, and B. Zhao, "Optimization of ultrasonic circulating extraction of polysaccharides from Asparagus officinalis using response surface methodology," *Int. J. Biol. Macromol.*, vol. 49, no. 2, pp. 181–187, 2011, doi: 10.1016/j.ijbiomac.2011.04.012.

[35] A. K. Hassan, M. M. Rahman, G. Chattopadhay, and R. Naidu, "Kinetic of the degradation of sulfanilic acid azochromotrop (SPADNS) by Fenton process coupled with ultrasonic irradiation or L-cysteine acceleration," *Environ. Technol. Innov.*, vol. 15, 2019, doi: 10.1016/j.eti.2019.100380.

[36] E. GilPavas, I. Dobrosz-Gómez, and M. Á. Gómez-García, "Optimization and toxicity assessment of a combined electrocoagulation, H2O2/Fe2+/UV and activated carbon adsorption for textile wastewater treatment," *Sci. Total Environ.*, vol. 651, pp. 551–560, 2019, doi: 10.1016/j.scitotenv.2018.09.125.

[37] Z. Manaa, D. Chebli, A. Bouguettoucha, H. Atout, and A. Amrane, "Low-Cost Photo-Fenton-Like Process for the Removal of Synthetic Dye in Aqueous Solution at Circumneutral pH," *Arab. J. Sci. Eng.*, vol. 44, no. 12, pp. 9859–9867, 2019, doi:

10.1007/s13369-019-04101-4.

[38] J. Domenzain-Gonzalez, J. J. Castro-Arellano, L. A. Galicia-Luna, and L. Lartundo-Rojas, "Photo-Fenton Degradation of RB5 Dye in Aqueous Solution Using Fe Supported on Mexican Natural Zeolite," *Int. J. Photoenergy*, vol. 2019, 2019, doi: 10.1155/2019/4981631.

[39] K. M. Reza, A. Kurny, and F. Gulshan, "Photocatalytic Degradation of Methylene Blue by Magnetite+H2O2+UV Process," *Int. J. Environ. Sci. Dev.*, vol. 7, no. 5, pp. 325–329, 2016, doi: 10.7763/ijesd.2016.v7.793.